Catalysis Science & Technology

ROYAL SOCIETY OF CHEMISTRY

PAPER

View Article Online
View Journal | View Issue



Check for updates

Cite this: *Catal. Sci. Technol.*, 2024, 14, 6524

# Switching of selectivity from benzaldehyde to benzoic acid using MIL-100(V) as a heterogeneous catalyst in aerobic oxidation of benzyl alcohol†

Duygu Hacıefendioğlu [ab] and Ali Tuncel *[a]

Received 5th July 2024,
Accepted 24th September 2024

DOI: 10.1039/d4cy00832d

rsc.li/catalysis

A vanadium-centered metal organic framework [MIL-100(V)] was synthesized as a heterogeneous catalyst allowing the selectivity to be switched from almost quantitative formation of benzaldehyde (Bz-CHO) to quantitative formation of benzoic acid (Bz-COOH) by changing only the temperature in the aerobic oxidation of benzyl alcohol (Bz-OH). The aerobic oxidation of Bz-OH was performed using molecular oxygen or air in the temperature range of 60–120 °C. A Bz-CHO formation yield of 98.1% was obtained with quantitative Bz-OH conversion at 80 °C. When the oxidation temperature was set to 100 °C, a Bz-COOH formation yield of 100% was achieved with quantitative Bz-OH conversion. The suitability of a serial reaction mechanism including Bz-CHO formation from Bz-OH and Bz-COOH formation from Bz-CHO as the first and second stage reactions, respectively was investigated for the aerobic oxidation process. The apparent first-order rate constants determined for first and second stage reactions demonstrated that the first-stage reaction was faster with respect to the second one. The proposed kinetic model allowed the calculation of apparent activation energies for Bz-CHO formation from Bz-OH and Bz-COOH formation from Bz-CHO as 77.3 and 149.2 kJ mol$^{-1}$, respectively. The presence of hydroxyl (·OH) and superoxide anion ($O_2^{\cdot-}$) radicals in the aerobic oxidation was demonstrated by radical scavenging runs. A mechanism was proposed based on the crystalline structure of MIL-100(V) and the radical types identified by the scavenging runs. This study opens a new path for tuning of selectivity towards Bz-CHO or Bz-COOH, for the first time, using a transition metal based catalyst synthesized by a one-pot hydrothermal reaction.

## 1. Introduction

Metal organic framework (MOF) based heterogeneous catalysts with different active sites have been widely used for oxidation of benzyl alcohol (Bz-OH) with various oxidation agents.[1–14] MOFs with different metal centers such as Co, Zn, Ni, and Cu were used in Bz-OH oxidation leading to benzaldehyde (Bz-CHO) as the main product with a Bz-OH conversion of 81.8% and high selectivity (>99%).[1] Fe-anchored MOF-808 was evaluated as a catalyst for selective oxidation of Bz-OH to Bz-CHO at 90 °C, with a Bz-OH conversion of 99% and a Bz-CHO selectivity of 96%.[15] Flowerlike high-entropy oxide nanosheets (HEO-600) with a high surface area and high oxygen vacancy provided a Bz-CHO yield of 92.3% in the aerobic oxidation of Bz-OH at 110 °C in 1 h.[16]

The nanomaterials carrying vanadium based active sites are among the most widely used heterogeneous catalysts for catalytic or photocatalytic conversion of Bz-OH to Bz-CHO with high selectivity.[17–26] MOFs decorated with vanadium containing active sites have been found in this family.[27–30] Vanadium oxide (VOx) species supported on Zr-NU-1000 and Hf-MOF-808 MOFs and a mixed-valence polyoxovanadate-based MOF were used for selective oxidation of Bz-OH to Bz-CHO.[27–29] Monomolecular $VB_2$-doped MOFs were also successfully evaluated for photocatalytic oxidation of Bz-OH to Bz-CHO.[30]

The tuning of product selectivity is still a challenge in the oxidation of Bz-OH using molecular oxygen or various chemical oxidation agents. In most of the Bz-OH oxidation studies, Bz-CHO or Bz-COOH is targeted as the main product using a certain heterogeneous catalyst. While obtaining Bz-CHO as the main product, Bz-COOH or other by-products such as benzyl benzoate (Bz-BzO) may form with lower concentrations. A similar situation is also observed when Bz-COOH is obtained as the main product due to the formation

[a] Hacettepe University, Chemical Engineering Department, Ankara, Turkey. E-mail: atuncel@hacettepe.edu.tr
[b] Hacettepe University, Graduate School of Science and Engineering, Chemical Engineering Department, Ankara, Turkey

† Electronic supplementary information (ESI) available. See DOI: https://doi.org/10.1039/d4cy00832d

of other by-products. Recently, electrocatalytic oxidation (ECO) of benzyl alcohol has been proposed as an efficient tool for obtaining Bz-COOH as the main product with high Bz-OH conversion and high selectivity.[31–41]

Various heterogeneous catalysts were developed to achieve high Bz-COOH formation yield *via* chemical oxidation of Bz-OH using an oxidation agent.[42–47] The conversion of Bz-OH to Bz-COOH with a selectivity higher than 99% and overall conversion higher than 90% was achieved under dilute alkaline conditions using $W_{18}O_{49}$/holey ultrathin g-$C_3N_4$ nanosheets in visible light driven photocatalytic oxidation of Bz-OH.[42] Holey lamellar high-entropy oxide allowed achievement of 98% Bz-OH conversion with a Bz-COOH selectivity of 50% and a Bz-CHO selectivity of 29% in solvent-free aerobic oxidation of Bz-OH at 120 °C in a reaction period of 2 h.[43] It was also demonstrated that solvent- and ligand-free aerobic oxidation of Bz-OH was catalyzed by soluble/MOF-supported palladium single atoms with a Bz-COOH formation yield of 73% at 150 °C.[44] Silver-carrying polyoxotungstate frameworks provided 99% Bz-COOH selectivity with 99% Bz-OH conversion in photocatalytic aerobic oxidation of Bz-OH.[45] A Bz-COOH selectivity of 94.8% was obtained with 98.6% Bz-OH conversion using a metal–organic complex synthesized from Co(II) and azoamide-pyridyl and benzenetricarboxylate at 90 °C.[46] The Pd/1D-$TiO_2$ catalyst with ultralow Pd-content allowed the main product to be changed from >90% Bz-CHO to >60% Bz-COOH in photothermocatalytic aerobic oxidation of Bz-OH in the temperature range of 90–120 °C.[47]

On the other hand, the tuning of selectivity towards Bz-CHO or Bz-COOH was achieved by changing reaction conditions in the visible light driven photocatalytic oxidation of Bz-OH.[48,49] An S-scheme heterojunction with bimetallic oxide quantum dots and nitrogen-deficient conjugated polymers ($Ni_{0.5}Fe_{0.5}O$ QD/g-$C_3N_4$) provided Bz-OH conversions of 85% and 88% for Bz-CHO and Bz-COOH, respectively in the visible light driven photocatalytic oxidations performed by changing the oxidation medium.[48] The host–guest chemistry of porphyrin-based metallacages was evaluated to regulate ROS generation and to control the selective photocatalytic oxidation of Bz-OH.[49] So, Bz-OH was oxidized into Bz-CHO by the irradiation of oxidation medium containing a metallacage, while it was oxidized to Bz-COOH when the metallacage-C70 complex was included as a photosensitizer in the oxidation medium.[49] Oxygen vacancy rich $Bi_2MoO_6$ hollow microspheres were used as a photocatalyst in the oxidation of Bz-OH under simulated sunlight with Bz-CHO production rates up to 1310 mol $g^{-1}$ $h^{-1}$.[50] $Fe_3O_4$@CdS@CQDs nanostructure used as a photocatalyst for selectively converting Bz-OH to Bz-CHO provided production rates up to 57.22 mmol $g^{-1}$ $h^{-1}$.[51] Bz-CHO production rates up to 99.25 mmol $g^{-1}$ $h^{-1}$ were also achieved using amphiphilic $Bi_2WO_6$ microspheres in the aerobic oxidation of Bz-OH conducted in a biphasic system under simulated sunlight.[52]

According to the best of the author's knowledge, only one study reported that a Bz-COOH yield of 96% and a Bz-CHO yield of 93% were consecutively achieved by changing the temperature between 90° and 50 °C and by adjusting the feed flow rate in a continuous packed bed reactor including Pt black/$SiO_2$ (*i.e.* a commercial catalyst) using $H_2O_2$ as the oxidant in the oxidation of Bz-OH.[53] In the present work, MIL-100(V) was synthesized by the hydrothermal reaction of the vanadium precursor ($VCl_3$) with the organic linker triethyl-1,3,5-benzenetricarboxylate (TE-BTC). MIL-100(V) was evaluated as a heterogeneous catalyst for aerobic oxidation of Bz-OH in the temperature range of 80–120 °C. Bz-CHO was obtained as the main product with a formation yield of 98.1% and quantitative Bz-OH conversion at 80 °C. On the other hand, Bz-COOH was obtained as the main product with quantitative formation yield and quantitative Bz-OH conversion at 100 °C. Most of the heterogeneous catalysts developed for aerobic oxidation of Bz-OH at temperatures higher than 80 °C and also the photocatalysts used in simulated sunlight driven Bz-OH oxidations at room temperature allowed the synthesis of only Bz-CHO or only Bz-COOH with high formation yields and high selectivities. In the present work, MIL-100(V) was proposed as a transition metal-based catalyst allowing the selectivity and also the oxidation reaction to be switched by changing the temperature alone, and production of only Bz-CHO or only Bz-COOH with high selectivity at different oxidation temperatures. The present work opened a new path for tuning the selectivity towards Bz-CHO or Bz-COOH, using an inexpensive transition metal based catalyst synthesized by a facile, one-pot hydrothermal reaction and eliminated the product selectivity problem in the aerobic oxidation of Bz-OH.

## 2. Experimental

### 2.1 Materials

1,3,5-Benzene tricarboxylic acid (BTC, 98%), vanadium chloride ($VCl_3$, 97%), absolute ethanol, and concentrated sulphuric acid (95–98%) were purchased from Sigma-Aldrich Co., St. Louis, MO, U.S.A. for the synthesis of MIL-100(V). Deionized (DI) water was obtained from Direct-Q3 UV system (Millipore S.A.S, France, 18 MΩ). Anhydrous benzyl alcohol (≥99%) and anhydrous diethylene glycol dimethyl ether (DEGDME, 99.5%) were supplied from Sigma-Aldrich. The radical scavengers L-ascorbic acid (L-AA), isopropyl alcohol (IPA) and $NaN_3$ were also obtained from Sigma-Aldrich.

### 2.2 Synthesis of TE-BTC

To obtain the organic linker triethyl-1,3,5-benzenetricarboxylate (TE-BTC), the Fischer esterification reaction was carried out with alcohol and an acid catalyst as reported earlier.[54] 1,3,5-Benzene tricarboxylic acid was dissolved in 100 mL of absolute ethanol and 2 mL of sulphuric acid. The solution was refluxed at 80 °C for 8 h. After the reaction, the clear solution was naturally

cooled down to room temperature and a white precipitate formed during the cooling. The crude product was washed with cold DI water and dried at 60 °C for 24 h. The product was obtained with nearly 90% yield based on BTC.

### 2.3 Synthesis of MIL-100(V)

The obtained TE-BTC and the vanadium precursor ($VCl_3$) were dissolved in DI water (5 mL) with a molar ratio of 2 : 1. The synthesis of MIL-100(V) was carried out in a Teflon-lined hydrothermal reactor (100 mL) at 220 °C for 72 h under autogenous pressure. The reactor was naturally cooled down to room temperature and the green product was washed with EtOH and DI water, by successive centrifugation–decantation. Then, MIL-100(V) was dried at 60 °C for 24 h.

### 2.4 Catalyst characterization

The morphological properties of MIL-100(V) nanoparticles were determined by Scanning Electron Microscopy (SEM, Tescan, Czech Republic). The porous characteristics of MIL-100(V) were analyzed by nitrogen physisorption, using the BET equation (Quantachrome, Nova 2200E, UK). The crystalline structure of MIL-100(V) was investigated by X-ray diffraction spectroscopy (Panalytical Empyrean XRD, UK). X-ray photoelectron spectroscopy (K-Alpha XPS, Thermo Fischer Scientific, U.S.A.) was used for the determination of valence states of V, O and C on the surface of MIL-100(V) nanoparticles.

### 2.5 Aerobic oxidation of benzyl alcohol

A three-neck round bottom flask was used to investigate the activity of MIL-100(V) as a heterogeneous catalyst in the aerobic oxidation of Bz-OH. Unless stated otherwise diethylene glycol dimethyl ether (2.5 mL) and Bz-OH (20 μL) were mixed using a magnetic stirrer. For the production of Bz-CHO, typically, the solution was heated to 80 °C, then MIL-100(V) (80 mg) was introduced to the solution and molecular oxygen or air was fed as the oxidant with a flow rate of 15 mL $min^{-1}$ and 75 mL $min^{-1}$, respectively. For the production of Bz-COOH, typically, the solution was heated to 100° or 120 °C, MIL-100(V) (20 mg) was introduced to the solution and molecular oxygen or air was fed with a flow rate of 15 mL $min^{-1}$ and 75 mL $min^{-1}$, respectively.

Liquid samples were taken from the reactor at different times. The catalyst was filtered off and the clear solution was analyzed in a high-performance liquid chromatography (HPLC) system (SPD-10AV, Shimadzu, Japan) equipped with a UV-vis detector operated at 214 nm and a Phenomenex SphereClone column (C-18, 5 μm Silica, 250 × 4.60 mm). The conversion of Bz-OH and the selectivity to products were calculated as follows:

Conversion of Bz-OH,

$$C_T\ (\%) = [n_{\text{Bz-OH}}(0) - n_{\text{Bz-OH}}(t)]/n_{\text{Bz-OH}}(0) \times 100 \quad (1)$$

Selectivity,

$$S_{\text{Bz-CHO}} \text{ or } S_{\text{Bz-COOH}}\ (\%) = n_{\text{Main product}}/[n_{\text{Bz-OH}}(0) - n_{\text{Bz-OH}}(t)] \times 100 \quad (2)$$

where $n_{\text{Bz-OH}}(0)$ is the initial mole of Bz-OH introduced to the reaction medium, $n_{\text{Bz-OH}}(t)$ is the mole of unconverted Bz-OH at the time period, $t$ and $n_{\text{Main product}}$ is the mole of the main product formed (Bz-CHO or Bz-COOH).

## 3. Results and discussion

### 3.1 Characterization of MIL-100(V)

The schematic representation of the chemical route followed for the synthesis of MIL-100(V) is given in Fig. 1. In the first stage, TE-BTC was synthesized by the Fischer esterification reaction between BTC and ethanol in an acidic medium.[54] Then, MIL-100(V) was obtained by a hydrothermal reaction between the selected vanadium precursor ($VCl_3$) and TE-BTC at 220 °C. The SEM photographs of MIL-100(V) are given in Fig. 2A. As seen here, MIL-100(V) was in the form of irregular crystals roughly ranging between 100 and 500 nm in size. The hysteresis in the nitrogen adsorption/desorption isotherms given in Fig. 2B(i) obeyed the type-IV isotherm dominantly indicating a mesoporous structure. The pore-size distribution curve is given in Fig. 2B(ii). A narrow pore size distribution falling in the size range of 3.1–4.1 was observed with a mode pore size of 3.5 nm. The specific surface area of MIL-100(V) was determined as 373.6 $m^2\ g^{-1}$. The X-ray diffraction spectrum given in Fig. 2B(iii) confirmed the crystalline structure of MIL-100(V) and was consistent with the those of previously synthesized MIL-100(V) samples.[54–56] As previously described, MIL-100(V) is a vanadium(III) tricarboxylate containing oxo-centered trimers of $VO_6$ octahedra linked to the same vertex $\mu_3$-O.[54] The trimers are connected by 1,3,5-phenyl triethylcarboxylate moieties termed as supertetrahedra represented by a hybrid structure containing four trimers and four organic ligands. It should be also noted that MIL-100(V) is isostructural with MIL-100(Cr) and the XRD pattern of MIL-100(V) is consistent with the simulated MIL-100(Cr).[54,55]

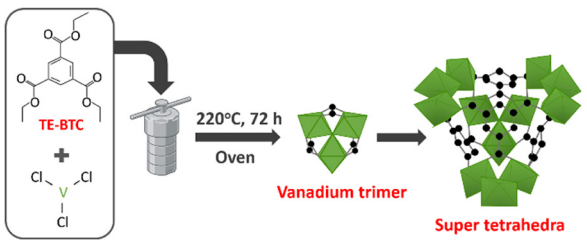


Fig. 1 Schematic representation of the chemical route followed for the synthesis of MIL-100(V).

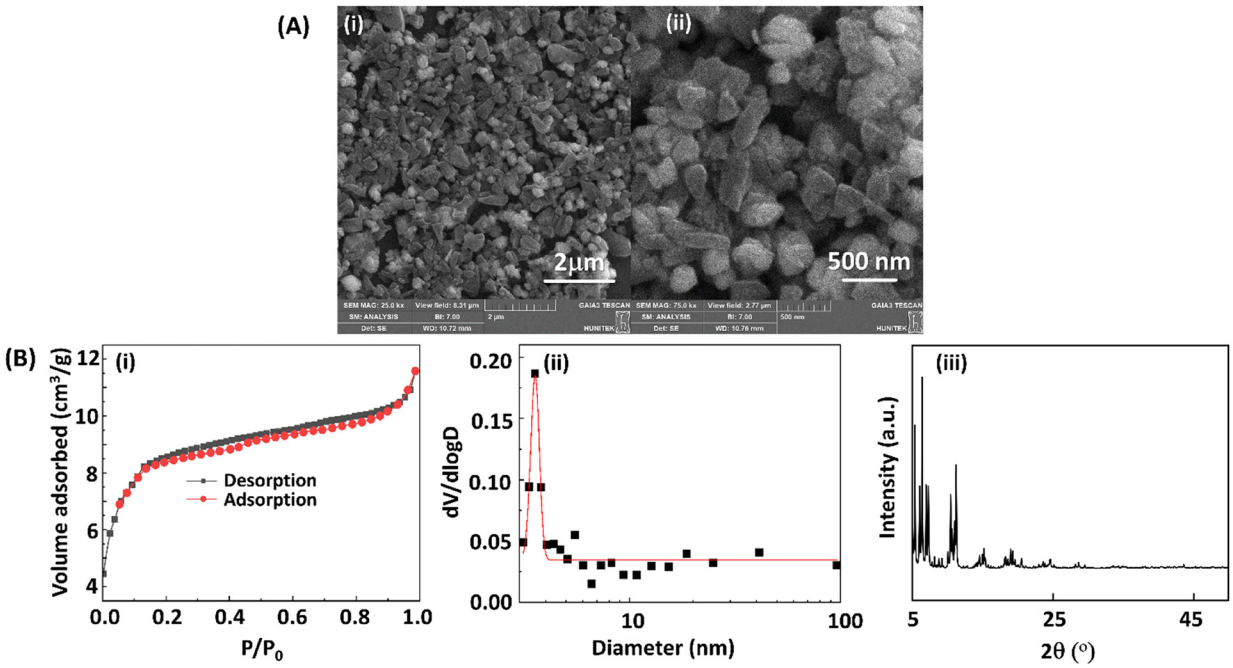


Fig. 2 Characterization of MIL-100(V). (A) SEM photographs of MIL-100(V). Magnification: ×25.000 and ×75.000 for (i) and (ii), respectively. (B) (i) Nitrogen adsorption/desorption isotherms of MIL-100(V), (ii) pore size distribution curve obtained by the nitrogen adsorption/desorption method, and (iii) X-ray diffraction spectrum of MIL-100(V).

X-ray photoelectron spectra of MIL-100(V) are presented in Fig. 3. The peaks belonging to V, O and C were observed in the survey XPS spectrum in Fig. 3A. In the core level spectra for the V 2p scan, the peaks assigned to V(III) and V(IV) valence states in the V $2p^{3/2}$ level were observed at binding energies of 517.01 and 517.78 eV, respectively (Fig. 3B). The peaks at binding energies of 521.17 and 523.34 eV were assigned to V(III) and V(IV) valence states in the V $2p^{1/2}$ level. V(III)/V(IV) mixed valence states were observed in the core level spectra for the V 2p scan of MIL-100(V). The V(III)/V(IV) ratio was calculated as 0.47 based on the peak areas obtained for V $2p^{3/2}$ and V $2p^{1/2}$ levels (Fig. 3B). The deconvoluted peaks at binding energies of 285.40, 286.66, 289.28 and 291.21 eV in the core level spectra for the C 1s scan were assigned to C–C, C–O, C═O and O–C═O, groups, respectively (Fig. 3C). In the core level spectra for the O 1s scan, the deconvoluted peaks at binding energies of 532.38, 532.83, and 538.40 eV were

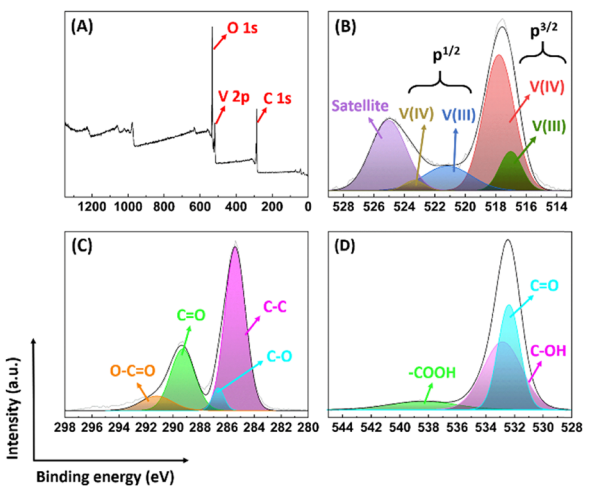


Fig. 3 X-ray photoelectron spectra (XPS) of MIL-100(V). (A) Survey XPS and core level spectra for (B) V 2p scan, (C) C 1s scan and (D) O 1s scan of MIL-100(V).

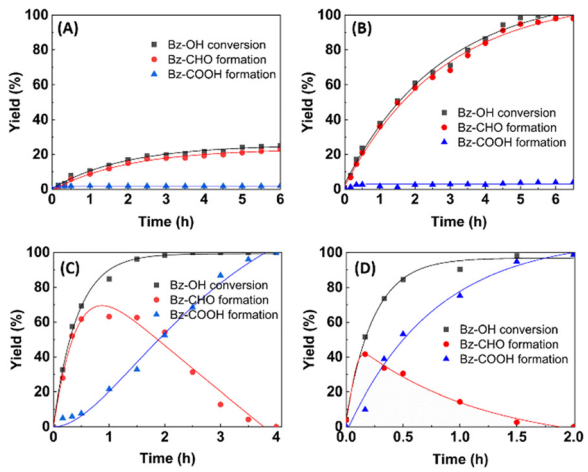


Fig. 4 Tuning of selectivity towards Bz-CHO or Bz-COOH by changing the reaction temperature in the presence of MIL-100(V) as a heterogeneous catalyst in the oxidation of Bz-OH with molecular oxygen. Reaction temperature (°C): (A) 60, (B) 80, (C) 100, (D) 120. Common conditions: DEGDME: 2.5 mL, MIL-100(V) concentration: 32 mg $mL^{-1}$, initial Bz-OH concentration: 96.2 mM, $O_2$ flow rate: 0.015 L $min^{-1}$.

**Table 1** Benzyl alcohol conversions, selectivities and formation yields of products obtained in the parametric runs made for aerobic oxidation of benzyl alcohol using MIL-100(V)

| Catalyst (mg mL$^{-1}$) | Temperature (°C) | $C_T$ (%) | $S_{Bz\text{-}CHO}$ (%) | $FY_{Bz\text{-}CHO}$ (%) | $S_{Bz\text{-}COOH}$ (%) | $FY_{Bz\text{-}COOH}$ (%) | TOF (h$^{-1}$) |
|---|---|---|---|---|---|---|---|
| 32 | 60 | 25.2 ± 2.2 | 92.6 ± 2.1 | 23.3 ± 2.1 | 7.4 ± 2.7 | 1.9 ± 2.7 | 3.3 |
| 32 | 80 | 100[a] | 98.1 ± 1.2 | 98.1 ± 1.2 | 3.0 ± 1.1 | 3.0 ± 1.1 | 18.4 |
| 32 | 100 | 100[a] | <0.1[b] | <0.1[b] | 99.9 ± 0.9 | 99.9 ± 0.9 | 18.0 |
| 32 | 120 | 100[a] | <0.1[b] | <0.1[b] | 98.8 ± 1.2 | 98.8 ± 1.2 | 62.9 |
| Catalyst (mg mL$^{-1}$) | Temperature (°C) | $C_T$ (%) | $S_{Bz\text{-}CHO}$ (%) | $FY_{Bz\text{-}CHO}$ (%) | $S_{Bz\text{-}COOH}$ (%) | $FY_{Bz\text{-}COOH}$ (%) | TOF (h$^{-1}$) |
| 8 | 80 | 93.7 ± 2.0 | 83.6 ± 1.4 | 78.3 ± 1.4 | 12.3 ± 1.7 | 13.4 ± 1.7 | 43.5 |
| 16 | 80 | 100[a] | 90.5 ± 1.1 | 90.5 ± 1.1 | 9.4 ± 1.0 | 9.4 ± 1.0 | 24.4 |
| 32 | 80 | 100[a] | 98.1 ± 1.2 | 98.1 ± 1.2 | 3.0 ± 1.1 | 3.0 ± 1.1 | 18.4 |
| 8 | 120 | 100[a] | <0.1[b] | <0.1[b] | 100.3 ± 1.9 | 100.3 ± 1.9 | 256.8 |
| 16 | 120 | 100[a] | <0.1[b] | <0.1[b] | 99.9 ± 1.6 | 99.9 ± 1.6 | 89.5 |
| 32 | 120 | 100[a] | <0.1[b] | <0.1[b] | 98.8 ± 1.2 | 98.8 ± 1.2 | 62.9 |
| Bz-OH (mM) | Temperature (°C) | $C_T$ (%) | $S_{Bz\text{-}CHO}$ (%) | $FY_{Bz\text{-}CHO}$ (%) | $S_{Bz\text{-}COOH}$ (%) | $FY_{Bz\text{-}COOH}$ (%) | TOF (h$^{-1}$) |
| 48.1 | 80 | 100[a] | 97.1 ± 0.8 | 97.1 ± 0.8 | 2.9 ± 1.2 | 2.9 ± 1.2 | 17.0 |
| 96.2 | 80 | 100[a] | 98.1 ± 1.2 | 98.1 ± 1.2 | 3.0 ± 1.1 | 3.0 ± 1.1 | 18.4 |
| 192.4 | 80 | 100[a] | 63.4 ± 1.3 | 63.4 ± 1.3 | 35.7 ± 1.7 | 35.7 ± 1.7 | 68.3 |
| 48.1 | 120 | 100[a] | <0.1[b] | <0.1[b] | 100.1 ± 1.7 | 100.1 ± 1.7 | 250.6 |
| 96.2 | 120 | 100[a] | <0.1[b] | <0.1[b] | 100.3 ± 1.9 | 100.3 ± 1.9 | 256.8 |
| 192.4 | 120 | 100[a] | <0.1[b] | <0.1[b] | 101.0 ± 1.5 | 101.0 ± 1.5 | 497.0 |
| Air flow rate (L min$^{-1}$) | Temperature (°C) | $C_T$ (%) | $S_{Bz\text{-}CHO}$ (%) | $FY_{Bz\text{-}CHO}$ (%) | $S_{Bz\text{-}COOH}$ (%) | $FY_{Bz\text{-}COOH}$ (%) | TOF (h$^{-1}$) |
| 0.050 | 80 | 61.1 ± 1.5 | 94.5 ± 1.4 | 57.8 ± 1.4 | 5.8 ± 1.6 | 3.6 ± 1.6 | 7.4 |
| 0.075 | 80 | 73.3 ± 1.6 | 95.5 ± 0.8 | 70.0 ± 0.8 | 5.6 ± 1.3 | 4.9 ± 1.3 | 9.74 |
| 0.150 | 80 | 100[a] | 92.1 ± 1.1 | 92.1 ± 1.1 | 8.3 ± 2.3 | 8.3 ± 2.3 | 19.9 |
| 0.050 | 120 | 100[a] | <0.1[b] | <0.1[b] | 99.7 ± 1.5 | 99.7 ± 1.5 | 121.8 |
| 0.075 | 120 | 100[a] | <0.1[b] | <0.1[b] | 99.0 ± 1.7 | 99.0 ± 1.7 | 207.3 |
| 0.150 | 120 | 100[a] | <0.1[b] | <0.1[b] | 99.1 ± 2.7 | 99.1 ± 2.7 | 221.6 |

$C_T$: Bz-OH conversion, $S_{Bz\text{-}CHO}$: Bz-CHO selectivity, $FY_{Bz\text{-}CHO}$: formation yield of Bz-CHO, $S_{Bz\text{-}COOH}$: Bz-COOH selectivity, $FY_{Bz\text{-}COOH}$: formation yield of Bz-COOH, TOF: turnover frequency at a total conversion of 80%. [a] No peak belonging to Bz-OH was found in the HPLC chromatogram. [b] Bz-CHO peak was very small in the HPLC chromatogram.

assigned to C═O, C–OH and –COOH groups, respectively (Fig. 3D).

### 3.2 Tuning of selectivity in aerobic oxidation of Bz-OH using MIL-100(V)

The effect of temperature on the kinetic behavior of aerobic oxidation of Bz-OH using MIL-100(V) as the catalyst is given in Fig. 4. The calculated kinetic parameters (*i.e.* Bz-OH conversion, selectivities and formation yields of Bz-CHO and Bz-COOH) at different temperatures are given in Table 1. In Fig. 4, the tunable synthesis of Bz-CHO or Bz-COOH by changing the temperature in the oxidation of Bz-OH was exemplified. As expected, a remarkable increase was observed in TOF with increasing temperature (Table 1). Quantitative Bz-OH conversions were obtained at temperatures higher than 60 °C. The Bz-CHO formation yield and also Bz-CHO selectivity were equal to 98.1%, while the formation yield and the selectivity to Bz-COOH were only 3.0% at 80 °C (Table 1). The formation yield and the selectivity to Bz-COOH were 99.9%, while the Bz-CHO formation yield and Bz-CHO selectivity were lower than 0.1% at 100 °C (Table 1). A similar behavior for the formation yields and the selectivities to both products was also observed at 120 °C. In other words, quantitative Bz-OH conversions and almost quantitative Bz-COOH formation yields were obtained when the oxidation temperature was set to 100 or 120 °C. The results obtained by using MIL-100(V) in the aerobic oxidation of Bz-OH demonstrated that Bz-CHO was the main product at the oxidation temperature of 80 °C, while Bz-COOH was obtained as the main product when Bz-OH oxidation was carried out at 100° or 120 °C. In other words, the tunable synthesis of Bz-CHO or Bz-COOH with considerably higher formation yields with respect to those previously reported was achieved by changing the reaction temperature when MIL-100(V) was used as the heterogeneous catalyst (Fig. 4, Table 1).[48–53] Apart from a pioneering study on switchable synthesis of aldehydes and carboxylic acids from different alcohols in a continuous packed bed reactor containing zerovalent Pt black (*i.e.* a commercial catalyst obtained from N.E. CHEMCAT Co., Japan) immobilized on $SiO_2$ as the catalyst, a similar behavior has not been observed with any catalyst synthesized for Bz-OH oxidation.[53] In the referred work, a Bz-COOH yield of 96% and a Bz-CHO yield of 93% were consecutively achieved by changing the temperature between 90 and 50 °C and adjusting the feed flow rate in the continuous reactor system using $H_2O_2$ as the oxidant.[53] MIL-100(V) is a more inexpensive catalyst and provided better formation yields and

 

selectivities for either Bz-CHO and Bz-COOH in the aerobic oxidation of Bz-OH using molecular oxygen as the oxidant. It should be also noted that the switching of selectivity towards Bz-CHO or Bz-COOH was also recently demonstrated in two different studies by modifying the chemistry of the photocatalyst or by changing the oxidation medium in the photocatalytic oxidation of Bz-OH.[48,49] In our case, a tunable synthesis either for Bz-CHO or Bz-COOH only by changing the reaction temperature and by keeping constant all other oxidation conditions was demonstrated for the first time in the aerobic oxidation of Bz-OH performed at temperatures higher than 80 °C.

The effect of MIL-100(V) concentration on the kinetic behavior of Bz-OH oxidation is demonstrated at two different temperatures (*i.e.* 80 and 120 °C) in Fig. 5. As seen here, the formation yield of Bz-CHO continuously increased with increasing time, while a limited increase was observed in the formation yield of Bz-COOH at 80 °C. However, Bz-CHO was in the form of an intermediate at 120 °C and the formation yield of Bz-COOH continuously increased by the consumption of Bz-CHO at this temperature (Fig. 5B). Note that the consumption of Bz-CHO at 120 °C was faster with the highest MIL-100(V) concentration. The calculated kinetic parameters are given in Table 1. As seen in Fig. 5A and Table 1, 80 °C is the oxidation temperature suitable for the synthesis of Bz-CHO with high selectivity and high formation yield in a reaction period of 6 h. In this set, the highest Bz-CHO selectivity and also the highest Bz-CHO formation yield were obtained as 98.1% with quantitative Bz-OH conversion at the MIL-100(V) concentration of 32.0 mg $mL^{-1}$ (Table 1). The Bz-COOH formation yield in the Bz-OH oxidation performed with the catalyst concentration of 32 mg $mL^{-1}$, at 80 °C, was 3.0% for a reaction period of 6.5 h (Table 1). The Bz-COOH formation yield increased to 5.3% when the reaction period was extended to 10 h under the same conditions.

No significant Bz-BzO formation was detected in the same run in a reaction period of 10 h. The formation yield of Bz-COOH was obtained as 99.9% in the oxidation performed with the catalyst concentration of 32 mg $mL^{-1}$ at 100 °C, in a reaction period of 4 h (Table 1). The formation yield of Bz-BzO was also lower than 0.1% when the reaction period was extended up to 8 h under the same conditions.

On the other hand, Bz-COOH was obtained as the single product with the formation yield of 100% when the Bz-OH oxidation was performed at 120 °C with the MIL-100(V) concentration of 8.0 mg $mL^{-1}$ in a reaction period of 2 h (Fig. 5B and Table 1). In this run, the overall Bz-OH conversion was quantitative and the formation yield of Bz-CHO was lower than 0.1%. The formation yield of Bz-BzO was found to be lower than 0.1% when the reaction period was extended to 4 h. Hence, the selectivity for Bz-COOH was calculated as 100% (Table 1). The TOF calculated for MIL-100(V) concentration of 8.0 mg $mL^{-1}$ at 120 °C was considerably higher with respect to that calculated for 32.0 mg $mL^{-1}$ at the same reaction temperature (Table 1). For this reason, 8.0 mg $mL^{-1}$ was evaluated as an appropriate MIL-100(V) concentration for the synthesis Bz-COOH at 120 °C and used in the rest of the oxidation runs for obtaining Bz-COOH as the main product. Another aerobic oxidation performed at 140 °C was completed in 1.5 h, with quantitative Bz-OH conversion, a Bz-COOH formation yield of 100 ± 1.4% and a Bz-BzO formation yield lower than 0.1%.

The effect of initial Bz-OH concentration on the kinetic behavior of Bz-OH oxidation was also investigated at two different reaction temperatures (Fig. S1†). Bz-CHO formation yields and Bz-CHO selectivities higher than 97% are obtained with lower initial Bz-OH concentrations at 80 °C (*i.e.* 48.1 and 96.2 mM) in a reaction period of 6 h. For the reaction temperature of 120 °C, both Bz-OH conversion and Bz-COOH formation yield are almost independent of initial Bz-OH concentration. Quantitative Bz-OH conversions and quantitative Bz-COOH formation yields were obtained with all initial Bz-OH concentrations in a reaction period of 2.5 h (Table 1). The highest TOF in this study is obtained in this set as 497 $h^{-1}$ with the highest initial Bz-OH concentration of 192.4 mM. As expected, the TOF values obtained with all initial Bz-OH concentrations at the reaction temperature of 120 °C are higher than those calculated at 80 °C.

Bz-OH oxidation runs were also performed using air instead of molecular oxygen as the oxidant. For the center point of oxidation runs, the air flow rate was selected by

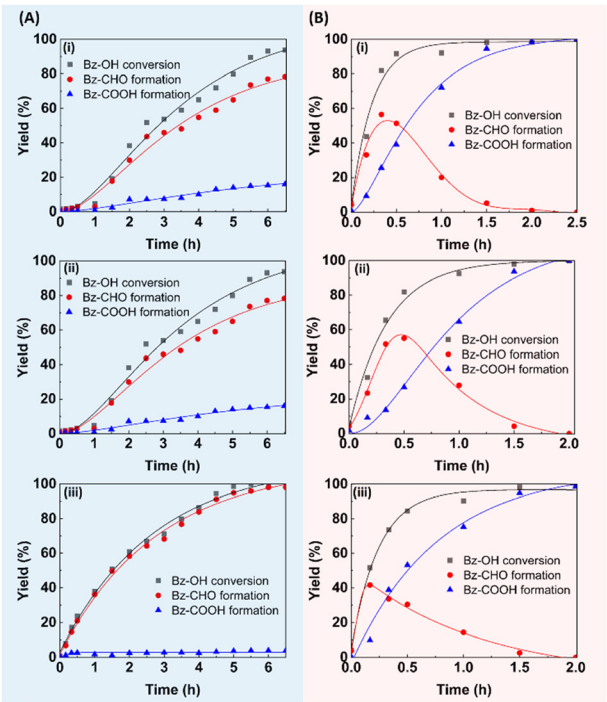


**Fig. 5** The variation of Bz-CHO and Bz-COOH formation with time in the Bz-OH oxidations performed by changing MIL-100(V) concentration at 80 °C and 120 °C, using molecular oxygen. (A) Bz-CHO and Bz-COOH formation profiles at 80 °C, MIL-100(V) concentration (mg $mL^{-1}$): (i) 8.0, (ii) 16.0, (iii) 32.0, (B) Bz-CHO and Bz-COOH formation profiles at 120 °C, MIL-100(V) concentration (mg $mL^{-1}$): (i) 8.0, (ii) 16.0, (iii) 32.0. Common conditions: DEGDME: 2.5 mL, initial Bz-OH concentration: 96.2 mM, $O_2$ flow rate: 0.015 L $min^{-1}$.

considering supplying oxygen with air at a flow rate which was equal to the flow rate of molecular oxygen. The effect of the air flow rate on the kinetic behavior of Bz-OH oxidation using MIL-100(V) as the catalyst is given in Fig. S2.† TOF values obtained using air at the reaction temperatures of 80 and 120 °C were lower with respect to the oxidation runs performed using molecular oxygen and by changing either catalyst concentration or initial Bz-OH concentration (Table 1). This finding indicated that the rate of Bz-OH oxidation leading to Bz-CHO or Bz-COOH as the main product using air was lower with respect to that performed using molecular oxygen. Quantitative Bz-OH conversion and high Bz-CHO formation yield (*i.e.* 92.1%) could be obtained with the highest air flow rate (0.15 L $min^{-1}$) at 80 °C. On the other hand, quantitative Bz-OH conversions and high Bz-COOH formation yields (*i.e.* >99%) were achieved with all air flow rates used at 120 °C.

The comparison of TOF values obtained for MIL-100(V) with the those of heterogeneous catalysts used in Bz-OH oxidation with different oxidation agents is given in Table S1.† Extremely high TOF values were reported for heterogeneous catalysts carrying precious metal nanoparticles as the active site on a porous support.[57–62] The TOF values obtained with MIL-100(V) were lower with respect to these catalysts. MIL-100(V) has an intrinsic catalytic activity in the oxidation of Bz-OH. For this reason, the mole of V used for TOF calculation of MIL-100(V) should be considerably higher with respect to the mole of precious metal used for TOF calculations of precious metal based catalysts. On the other hand, the TOF values obtained with MIL-100(V) were considerably higher with respect to catalysts containing various transition metals.[63–67] In Table S1,† all TOF values were taken from the studies on Bz-OH oxidations leading to Bz-CHO as the main product. For MIL-100(V), the TOF reported for 120 °C belongs to Bz-OH oxidation providing Bz-COOH with 100% selectivity, while the TOF reported for 80 °C defines Bz-CHO formation with 98.1% selectivity.

### 3.3 Kinetic analysis of aerobic oxidation of Bz-OH using MIL-100(V)

A serial reaction system was used for the kinetic analysis of aerobic oxidation of Bz-OH using MIL-100(V) as the catalyst (Fig. 6). Although similar reaction schemes including both Bz-CHO and Bz-COOH formations have been previously used in numerous studies, the estimation of apparent rate constants of individual reactions leading to Bz-CHO and Bz-COOH was not performed in both catalytic and photocatalytic Bz-OH oxidations.[42–53] The effective catalysis of Bz-CHO and Bz-COOH formation reactions by MIL-100(V) only by changing the oxidation temperature under constant reaction conditions allowed the kinetic analysis to be carried out as described below.

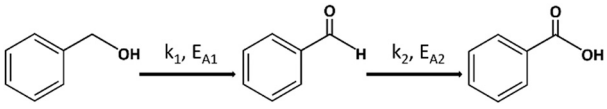


Fig. 6 The serial reaction system for aerobic oxidation of Bz-OH using MIL-100(V).

As seen in Fig. 6, Bz-CHO is obtained as the intermediate product by the first-stage reaction with the first order apparent rate constant of $k_1$. Then, Bz-COOH is obtained as the final product by the second reaction with the first order apparent rate constant of $k_2$. The first-order rate expression for the conversion of Bz-OH to Bz-CHO is given by eqn (3). Then, the expression for the variation of Bz-OH concentration with time is given by eqn (4).

$$-\frac{dC_{Bz\text{-}OH}}{dt} = k_1 C_{Bz\text{-}OH} \quad (3)$$

$$C_{Bz\text{-}OH} = C^0_{Bz\text{-}OH} \exp(-k_1 t) \quad (4)$$

The net reaction rate of Bz-CHO as the intermediate can be expressed by eqn (5) by considering either the formation or the decomposition rates. Hence, the expression for the variation of Bz-CHO concentration with time is obtained by the integration of eqn (5), using eqn (4). The formation rate of Bz-COOH is given by eqn (6) by considering the decomposition of Bz-CHO with the second reaction according to first-order kinetics. Finally, by substituting eqn (6) into eqn (7), the integration of the resulting expression yields eqn (8) for the variation of Bz-COOH concentration with time.

$$\frac{dC_{Bz\text{-}CHO}}{dt} = k_1 C_{Bz\text{-}OH} - k_2 C_{Bz\text{-}CHO} \quad (5)$$

$$C_{Bz\text{-}CHO} = \frac{k_1 C^0_{Bz\text{-}OH}}{k_2 - k_1}[\exp(-k_1 t) - \exp(-k_2 t)] \quad (6)$$

$$\frac{dC_{Bz\text{-}COOH}}{dt} = k_2 C_{Bz\text{-}CHO} \quad (7)$$

$$C_{Bz\text{-}COOH} = \left[\frac{k_2 C^0_{Bz\text{-}OH}}{k_1 - k_2}(\exp(-k_1 t) - 1) - \frac{k_1 C^0_A}{k_1 - k_2}(\exp(-k_2 t) - 1)\right] \quad (8)$$

A non-linear parameter estimation protocol *via* MATLAB® was used for the determination of apparent first order rate constants based on the variation of Bz-OH, Bz-CHO and Bz-COOH concentrations with time for each oxidation run as given in Fig. 4 and 5 and S1 and S2.† The first-order rate constants belonging to the first and second reactions in Fig. 6 are given in Table 2.

- The rate constants for Bz-COOH formation from Bz-CHO (*i.e.* $k_2$) are much lower with respect to those of Bz-CHO formation from Bz-OH (*i.e.* $k_1$) in all runs performed at 80 °C.
- The rate constants for Bz-CHO formation from Bz-OH and Bz-COOH formation from Bz-CHO are appreciably high in all aerobic oxidations performed at 120 °C. This finding clearly shows that either Bz-CHO formation from Bz-OH or Bz-COOH formation from Bz-CHO can be effectively catalyzed

 

Table 2 The apparent first order rate constants for the formation of Bz-CHO and Bz-COOH in the serial reaction system for aerobic oxidation of benzyl alcohol with MIL-100(V) as the catalyst

| Catalyst (mg mL$^{-1}$) | Temperature (°C) | $k_1$ (h$^{-1}$) | $k_2$ (h$^{-1}$) |
|---|---|---|---|
| 8 | 80 | 0.27 | 0.03 |
| 16 | 80 | 0.33 | 0.02 |
| 32 | 80 | 0.50 | 0.003 |
| 8 | 120 | 3.96 | 2.93 |
| 16 | 120 | 3.93 | 2.98 |
| 32 | 120 | 3.88 | 3.42 |
| **Bz-OH (mM)** | **Temperature (°C)** | $k_1$ (h$^{-1}$) | $k_2$ (h$^{-1}$) |
| 48.1 | 80 | 0.89 | 0.006 |
| 96.2 | 80 | 0.98 | 0.003 |
| 192.4 | 80 | 1.54 | 0.003 |
| 48.1 | 120 | 5.88 | 4.86 |
| 96.2 | 120 | 3.96 | 2.93 |
| 192.4 | 120 | 3.92 | 2.40 |
| **Air flow rate (L min$^{-1}$)** | **Temperature (°C)** | $k_1$ (h$^{-1}$) | $k_2$ (h$^{-1}$) |
| 0.050 | 80 | 0.14 | 0.002 |
| 0.075 | 80 | 0.40 | 0.003 |
| 0.150 | 80 | 0.59 | 0.020 |
| 0.050 | 120 | 1.95 | 0.79 |
| 0.075 | 120 | 3.67 | 1.87 |
| 0.150 | 120 | 3.87 | 1.92 |
| **Catalyst (mg mL$^{-1}$)** | **Temperature (°C)** | $k_1$ (h$^{-1}$) | $k_2$ (h$^{-1}$) |
| 32 | 60 | 0.06 | 0.002 |
| 32 | 80 | 0.50 | 0.003 |
| 32 | 100 | 2.33 | 0.59 |
| 32 | 120 | 3.88 | 3.42 |

$k_1$: apparent first order rate constant for Bz-CHO formation from Bz-OH, $k_2$: apparent first order rate constant for Bz-COOH formation from Bz-CHO.

by MIL-100(V) when the oxidation is conducted at a satisfactorily high temperature such as 120 °C. However, the rate constants obtained for Bz-CHO formation from Bz-OH are higher with respect to those for Bz-COOH formation from Bz-CHO for all runs given in Table 2. This finding indicates that the first reaction is faster with respect to the second one when MIL-100(V) is used as the heterogeneous catalyst.

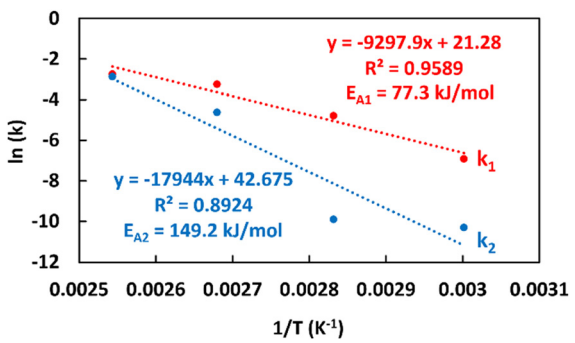


Fig. 7 Arrhenius plots of apparent first-order rate constants determined for Bz-CHO and Bz-COOH formations by the serial reaction system proposed for aerobic oxidation of Bz-OH using MIL-100(V).

- As expected, the apparent first order rate constants determined for either Bz-CHO formation or Bz-COOH formation increased with increasing temperature. The Arrhenius plots for both rate constants are given in Fig. 7. The apparent activation energies for Bz-CHO and Bz-COOH formation reactions in the serial reaction system were determined as 77.3 kJ mol$^{-1}$ and 149.2 kJ mol$^{-1}$, respectively. Note that the apparent activation energy calculated for Bz-COOH formation from Bz-CHO is almost two times higher with respect to that found for Bz-CHO formation from Bz-OH. This property is a factor involving the higher reaction rate for the catalytic reaction from Bz-OH to Bz-CHO. The surface of MIL-100(V) is covered with negatively charged carboxyl groups with hydrophilic character. The adsorption tendency of Bz-OH onto the hydrophilic surface of the catalyst is expected to be higher with respect to Bz-CHO since Bz-OH is more hydrophilic than Bz-CHO. The higher adsorption tendency of Bz-OH might be a factor involving the higher rate in the catalytic reaction from Bz-OH to Bz-CHO with respect to the catalytic reaction from Bz-CHO to Bz-COOH.
- When air is used as the oxidant instead of molecular oxygen, by using the same $O_2$ flow rate in the air flow, particularly, the rate constant for Bz-CHO formation from Bz-OH is lower with respect to the rate constant obtained with molecular oxygen under the same conditions at 80 °C. The values of rate constants both for first and second-stage reactions decreased when air was used as the oxidant at 120 °C.
- The results show that MIL-100(V) is a unique nanomaterial which is capable of catalyzing either Bz-CHO formation from Bz-OH or Bz-COOH formation from Bz-CHO in the aerobic oxidation of Bz-OH at the appropriate temperatures. This property has not been observed yet with the heterogeneous catalysts developed for catalytic, photocatalytic and electrocatalytic Bz-OH oxidations.

### 3.4 Radical scavenging runs in aerobic oxidation of Bz-OH with MIL-100(V)

In order to determine the radical types that were effective on Bz-CHO and Bz-COOH formation stages, radical scavenging runs were performed at 80° and 120 °C, respectively in the aerobic oxidation of Bz-OH catalyzed by MIL-100(V), using $O_2$ as the oxidant. In these runs, L-AA, IPA and $NaN_3$ were used as scavengers for singlet oxygen ($^1O_2$), hydroxyl (·OH) and superoxide anion ($O_2^{\bullet-}$) radicals, respectively. The concentration of each scavenger was set to 10 mM. The effects of different radical scavengers on the kinetic behavior of the Bz-OH oxidation system is given in Fig. S3† Bz-OH conversions, product selectivities and product formation yields obtained in the radical scavenging runs at 80° and 120 °C are given in Table 3.

As seen in Fig. S3† and Table 3, the Bz-CHO formation kinetics was not affected by L-AA, while serious inhibitions for Bz-CHO formation were observed in the presence of

Table 3 Benzyl alcohol conversions, selectivities and formation yields of products obtained in radical scavenging runs performed for aerobic oxidation of benzyl alcohol using MIL-100(V)

| Reaction conditions | Scavenger type | $C_T$ (%) | $S_{Bz\text{-}CHO}$ (%) | $FY_{Bz\text{-}CHO}$ (%) | $S_{Bz\text{-}COOH}$ (%) | $FY_{Bz\text{-}COOH}$ (%) | TOF ($h^{-1}$) |
|---|---|---|---|---|---|---|---|
| 32 mg $mL^{-1}$ 80 °C | No scavenger | 100[a] | 98.1 ± 1.2 | 98.1 ± 1.2 | 3.0 ± 1.1 | 3.0 ± 1.1 | 18.4 |
| | L-AA | 96.8 ± 1.7 | 95.9 ± 1.4 | 92.8 ± 1.4 | 4.5 ± 0.6 | 3.9 ± 0.6 | 18.4 |
| | IPA | 73.6 ± 1.2 | 86.8 ± 0.9 | 63.9 ± 0.9 | 8.8 ± 1.3 | 9.7 ± 1.3 | 8.9 |
| | $NaN_3$ | 84.5 ± 2.1 | 77.1 ± 1.4 | 65.1 ± 1.4 | 22.6 ± 1.7 | 19.4 ± 1.7 | 9.8 |
| 8 mg $mL^{-1}$ 120 °C | No scavenger | 100[a] | <0.1[b] | <0.1[b] | 100.3 ± 1.9 | 100.3 ± 1.9 | 256.8 |
| | L-AA | 100[a] | <0.1[b] | <0.1[b] | 100 ± 2.2 | 100 ± 2.2 | 245.3 |
| | IPA | 90.6 ± 1.8 | 49.3 ± 1.7 | 44.7 ± 1.7 | 50.7 ± 2.0 | 45.9 ± 2.0 | 110.1 |
| | $NaN_3$ | 75.1 ± 1.7 | 23.9 ± 1.8 | 17.9 ± 1.8 | 76.1 ± 2.4 | 57.2 ± 2.4 | 76.5 |

$C_T$: Bz-OH conversion, $S_{Bz\text{-}CHO}$: Bz-CHO selectivity, $FY_{Bz\text{-}CHO}$: formation yield of Bz-CHO, $S_{Bz\text{-}COOH}$: Bz-COOH selectivity, $FY_{Bz\text{-}COOH}$: formation yield of Bz-COOH, TOF: turnover frequency at a total conversion of 80%. [a] No peak belonging to Bz-OH was found in the HPLC chromatogram. [b] Bz-CHO peak was very small in the HPLC chromatogram.

IPA and $NaN_3$ at 80 °C. As also seen in both Fig. S3† and Table 3, Bz-COOH formation was seriously inhibited in the presence of IPA and $NaN_3$ at 120 °C, while no apparent change was observed in the Bz-COOH formation kinetics with respect to Bz-OH oxidation containing no scavenger at the same temperature. Note that the TOF values determined in the presence of IPA and $NaN_3$ at 80° and 120 °C were considerably lower with respect to the Bz-OH oxidations performed in the absence of these scavengers (Table 3). The apparent first-order rate constants in the radical scavenging runs determined according to the serial reaction system proposed for aerobic oxidation of Bz-OH with MIL-100(V) are given in Table 4. The apparent first-order rate constants determined with IPA and $NaN_3$ were considerably lower at both temperatures, with respect to those found for Bz-OH oxidations performed without using these scavengers (Table 4). Hence, the inhibition of Bz-CHO formation at 80 °C and the inhibition of Bz-COOH formation at 120 °C by either IPA or $NaN_3$ were confirmed by the apparent rate constants determined with these scavengers. All these findings clearly indicated that ·OH and $O_2^{\bullet-}$ radicals were strongly effective for Bz-CHO formation at 80 °C and Bz-COOH formation at 120 °C in the aerobic oxidation of Bz-OH catalyzed by MIL-100(V).

Table 4 The apparent first order rate constants in the radical scavenging runs analyzed according to the serial reaction system for aerobic oxidation of benzyl alcohol with MIL-100(V)

| Reaction conditions | Scavenger | $k_1$ ($h^{-1}$) | $k_2$ ($h^{-1}$) |
|---|---|---|---|
| 32 mg $mL^{-1}$ 80 °C | No scavenger | 0.50 | 0.003 |
| | L-AA | 0.47 | 0.003 |
| | IPA | 0.21 | 0.003 |
| | $NaN_3$ | 0.24 | 0.098 |
| 8 mg $mL^{-1}$ 120 °C | No scavenger | 3.96 | 2.93 |
| | L-AA | 3.81 | 2.11 |
| | IPA | 2.05 | 0.55 |
| | $NaN_3$ | 0.82 | 1.10 |

$k_1$: apparent first order rate constant for Bz-CHO formation from Bz-OH, $k_2$: apparent first order rate constant for Bz-COOH formation from Bz-CHO.

MIL-100(V) exhibits lower substrate adsorption since it possesses relatively weak Lewis acid centers available to the reactants compared with other MIL-100 type catalysts (*i.e.* MIL-100(Al), MIL-100(Fe), or MIL-100(Cr)).[54–56,68–70] Therefore the catalyst is resistant against poisoning or irreversible adsorption while preserving a satisfactorily high Bz-OH conversion rate with appropriate Bz-OH adsorption.[68] MIL-100(V) also has a high surface area and a large number of Lewis metal sites available to the reactants.[69,70] The observation of V(III) and V(IV) mixed valence states from core level spectra for the V 2p scan indicates the presence of coordinatively unsaturated metal sites (CUS) on the surface structure of MIL-100(V).[71] The combination of accessible metal sites with different oxidation states and the enhanced porous properties providing a large surface area should be likely responsible for the high catalytic activity of MIL-100(V) in the aerobic oxidation of Bz-OH.[72]

By considering the radicals which are effective on the aerobic oxidation of Bz-OH with MIL-100(V), a schematic description of the reaction mechanism is given in Fig. 8 for two different temperatures (*i.e.* 80° and 120 °C). The aerobic oxidation of Bz-OH with MIL-100(V) can be divided into three stages for Bz-CHO formation at 80 °C (Fig. 8A). The first stage is the adsorption of Bz-OH onto V(III)-CUSs to create $H^+$ and to release electrons. In the second stage, the reactive $H^+$ atoms merge with molecular oxygen to form ·OH radicals. The released electrons also attack molecular oxygen to form $O_2^{\bullet-}$ radicals. The last stage is the formation of Bz-CHO at 80 °C, and its desorption from the surface of MIL-100(V) (Fig. 8A). At temperatures higher than 80 °C (*i.e.* 100° or 120 °C), a similar reaction scheme also involving the participation of ·OH and $O_2^{\bullet-}$ radicals is also followed for further oxidation Bz-CHO to Bz-COOH started by the adsorption of Bz-CHO onto V(III)-CUSs (Fig. 8B).

### 3.5 Recyclability of MIL-100(V) in the aerobic oxidation of Bz-OH

The recyclability behavior of MIL-100(V) in the aerobic oxidation of Bz-OH conducted at two different

 

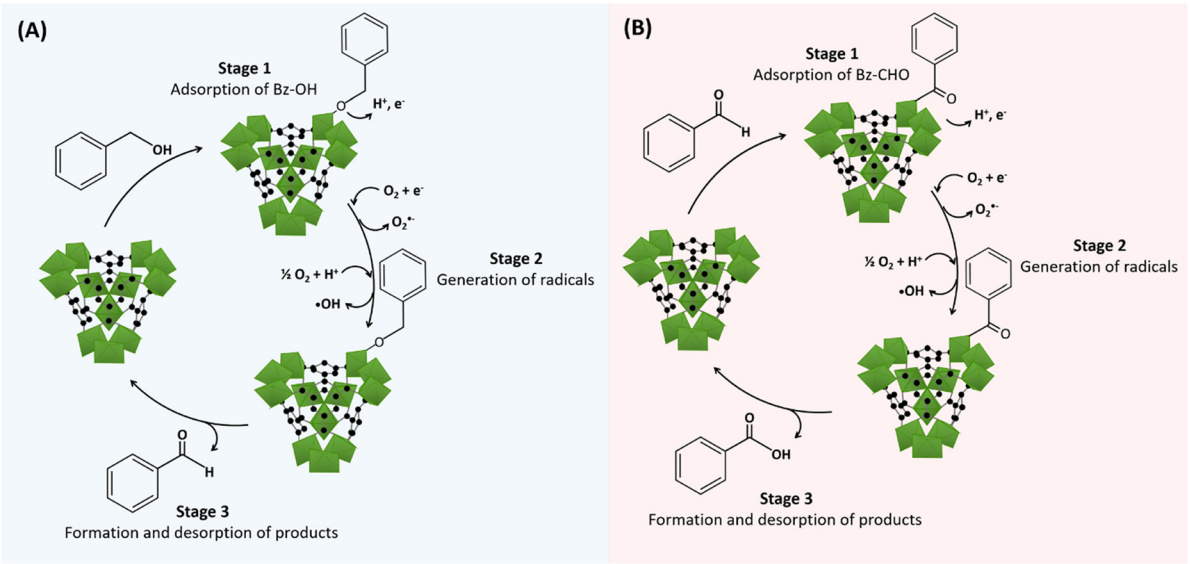


**Fig. 8** The reaction mechanism proposed based on the radical scavenging runs performed for aerobic oxidation of Bz-OH using MIL-100(V). (A) Bz-CHO formation and (B) Bz-COOH formation.

temperatures (*i.e.* 80 and 120 °C) is given in Fig. 9. The Bz-OH conversion and Bz-CHO formation yield decreased by 7.7% and 5.2%, respectively, over 5 consecutive oxidation runs performed at 80 °C. On the other hand, 3.3% lower Bz-OH conversion and 10.3% lower Bz-COOH formation yield were obtained over 5 consecutive oxidation runs conducted at 120 °C. MIL-100(V) exhibited a satisfactorily stable catalytic activity in the Bz-OH oxidation runs performed for obtaining Bz-CHO and Bz-COOH as the main products. No significant change was observed either in the morphology or crystalline structure of MIL-100(V) after using five consecutive oxidation runs performed at 80° and 120 °C (Fig. S4 and S5†). XPS spectra of MIL-100(V) samples obtained after 5 consecutive oxidation runs performed at 80° and 120 °C are given in Fig. S6.† V(III) and V(IV) valence states were also observed in the core level spectra for the V 2p scan of MIL-100(V) samples obtained after the recyclability runs performed for obtaining Bz-CHO and Bz-COOH (Fig. S6†). The V(III)/V(IV) ratio was calculated as 0.47 using the core level spectra for the V 2p scan of as-synthesized MIL-100(V) (Fig. 3A). V(III)/V(IV) ratios of MIL-100(V) samples used in the oxidation runs providing Bz-CHO and Bz-COOH as the main products were determined as 0.32 and 0.37, respectively using their core level spectra for the V 2p scan. This comparison indicated that the V(III) content of MIL-100(V) moderately decreased after being used in the Bz-OH oxidation runs made at 80° and 120 °C. The deconvoluted peaks belonging to the functional groups which were identical with those of unused MIL-100(V) were also observed in the core level spectra for the C 1s scan and O 1s scan recorded with MIL-100(V) samples obtained from the recyclability runs performed at either 80° or 120 °C (panel A and B in Fig. S6†).

## 4. Conclusion

In most of the oxidation processes used for Bz-OH, the oxidation protocol allows the synthesis of a single product with high selectivity. Bz-CHO is the main product in the oxidations performed using molecular oxygen or chemical oxidation agents at temperatures ranging between 80 and 120 °C. On the other hand, electrocatalytic oxidation is another approach providing Bz-COOH as the main product with high selectivity. A limited number of studies on the visible light driven photocatalytic oxidation of Bz-OH provided Bz-CHO or Bz-COOH with high yields by changing the chemical structure of the catalyst or the solvent used as the oxidation medium. In our case, MIL-100(V) is proposed as a heterogeneous catalyst allowing Bz-CHO or Bz-COOH to be obtained with almost quantitative yield and quantitative Bz-OH conversion by only changing the temperature performed using the same solvent and without changing the chemistry of the catalyst. Hence, the synthesized catalyst provided a new path to overcome the selectivity problem for either Bz-CHO or Bz-COOH in the aerobic oxidation of Bz-OH. Another superiority of MIL-100(V) is the simplicity of the synthesis protocol based on a one-pot reaction between $VCl_3$ as the metal precursor and triethyl-1,3,5-benzenetricarboxylate as the organic ligand. The intrinsic catalytic activity of MIL-100(V) in aerobic oxidation is another advantage. Oxidation rates with almost the same order of magnitude observed with precious metal based catalysts (such as $PdAu@SiO_2$ or $Pd@Mn_5O_8$ *etc.*) could be achieved using MIL-100(V) in the aerobic oxidation of Bz-OH. MIL-100(V) should have a lower production cost as a transition metal catalyst with respect to those containing noble metal based active sites. The evaluation of MIL-100(V) in the aerobic oxidation of alkylbenzenes such as toluene/ethylbenzene may also provide

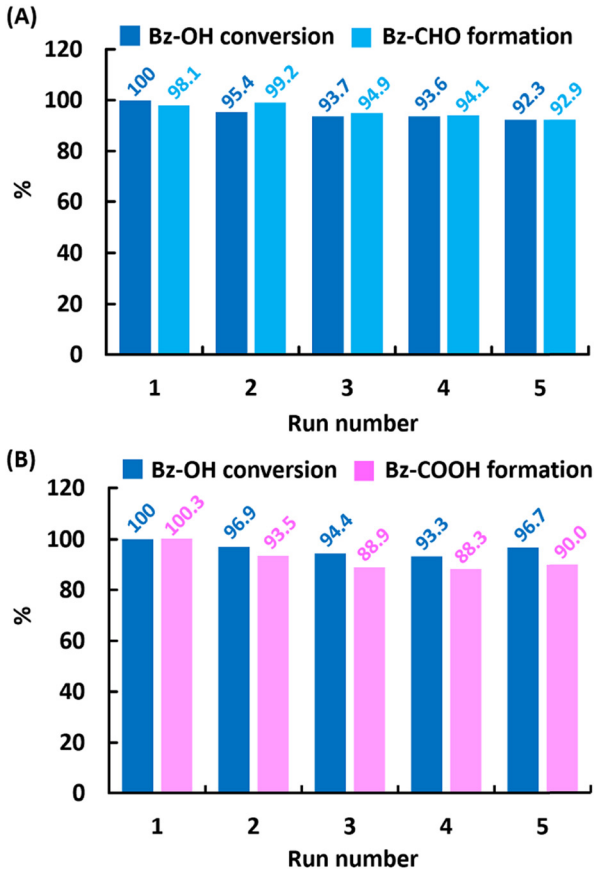


Fig. 9 (A) The variation of Bz-OH conversion and Bz-CHO formation yield with the run number in the recyclability runs performed at 80 °C. (B) The variation of Bz-OH conversion and Bz-COOH formation yield with the run number in the reusability runs performed at 120 °C. Common conditions: DEGDME: 2.5 mL, initial Bz-OH concentration: 96.2 mM, $O_2$ flow rate: 0.015 L $min^{-1}$, MIL-100(V) concentration for the runs performed at 80 °C: 32 mg $mL^{-1}$, MIL-100(V) concentration for the runs performed at 120 °C: 8 mg $mL^{-1}$.

interesting results by tuning the product selectivity in a broad spectrum. The synthesis of heterogeneous catalysts in the form of MIL-100 using triethyl-1,3,5-benzenetricarboxylate as the organic ligand with different metal precursors may also give heterogeneous catalysts for various organic reactions different than oxidation of alcohols.

## Data availability

The data supporting this article have been included as part of the ESI†

## Author contributions

Duygu Hacıefendioğlu: data curation, formal analysis, validation, visualization, investigation, methodology, software, writing – original draft. Ali Tuncel: resources, funding acquisition, conceptualization, supervision, investigation, methodology, project administration, writing – original draft, writing – review & editing.

## Conflicts of interest

There are no conflicts to declare.

## Acknowledgements

The authors thank Turkish Academy of Sciences (TUBA) for the research support provided to Prof. Ali Tuncel as a full member. The authors also thank M. Cihan Demir for his help in technical drawings.

## References

1 L. Peng, S. Wu, X. Yang, J. Hu, X. Hu, Q. Huo and J. Guan, *RSC Adv.*, 2016, **6**, 72433–72438.
2 L. Liu, X. Tai, X. Zhou, J. Hou and Z. Zhang, *J. Alloys Compd.*, 2019, **790**, 326–336.
3 A. Paul, L. M. D. R. S. Martins, A. Karmakar, M. L. Kuznetsov, A. S. Novikov, M. F. C. G. Silva and A. J. L. Pombeiro, *J. Catal.*, 2020, **385**, 324–337.
4 T. Guo, S. Bao, J. Guo, W. Chen and L. Wen, *Chem. Res. Chin. Univ.*, 2022, **38**, 134–1348.
5 M. Mohammadikish and M. Panahi, *CrystEngComm*, 2023, **25**, 5470–5478.
6 S. Javanbakht, R. Mohammadian, H. Farhid, A. Shaabani and M. M. Amini, *Mater. Today Commun.*, 2021, **28**, 102502.
7 S. Oudi, A. R. Oveisi, S. Daliran, M. Khajeh, R. Luque, U. Sen and H. Garcia, *Appl. Catal., A*, 2021, **611**, 117965.
8 Q. Zhang, J. B. Liu, L. Chen, C. X. Xiao, P. Chen, S. Shen, J. K. Guo, C. T. Au and S. F. Yin, *Appl. Catal., B*, 2020, **264**, 118529.
9 P. Li, X. Yan, S. Gao and R. Cao, *J. Chem. Eng.*, 2021, **421**, 129870.
10 Y. Qin, M. Hao, J. Wang, R. Yuan and Z. Li, *ACS Appl. Mater. Interfaces*, 2022, **14**, 56930–56937.
11 J. Liu, X. Sun, B. Jiang, M. Liu, Q. Li, X. Xiao, H. Wang, M. Zheng, S. Guo, J. Wu, Y. Zhang, K. Shi and W. Zhou, *ACS Appl. Nano Mater.*, 2022, **5**, 2231–2240.
12 D. L. Xie, S. A. Li, W. Q. Yang, S. L. Fan and Y. S. Feng, *ChemistrySelect*, 2022, **7**, e202103521.
13 M. Li, J. Qiu, J. Xu, Y. Zhu and J. Yao, *ACS Appl. Mater. Interfaces*, 2022, **14**, 11509–11516.
14 X. Z. Wei, F. W. Dagnaw, J. Liu and L. Ma, *J. Colloid Interface Sci.*, 2023, **629**, 136–143.
15 W. Jumpathong, T. Pila, Y. Lekjing, P. Chirawatkul, B. Boekfa, S. Horike and K. Kongpatpanich, *APL Mater.*, 2019, **7**, 111109.
16 B. Zhang, J. Chen, Y. Li, Y. Zhu, Y. Yang, S. Liao, W. Xiao, S. Wang, P. Zhang, Y. Shu, S. Shi and C. Chen, *ACS Appl. Nano Mater.*, 2023, **6**, 20310–20319.
17 B. Das, M. Sharma, M. J. Baruah, B. P. Mounash, G. V. Karunakar and K. K. Bania, *J. Environ. Chem. Eng.*, 2020, **8**, 104268.
18 L. Zhao, P. Yang, S. Shi, G. Zhu, X. Feng, W. Zheng, D. G. Vlachos and J. Xu, *ACS Catal.*, 2022, **12**, 15249–15258.

19 Y. Wu, L. H. Kong, W. T. Ge, W. J. Zhang, Z. Y. Dong, X. J. Guo, X. Yan, Y. Chen and W. Z. Lang, *J. Catal.*, 2022, **413**, 668–680.
20 E. V. Sabre, B. M. Viola, A. L. Canepa and S. G. Casuscelli, *Top. Catal.*, 2022, **65**, 1373–1381.
21 D. Gömpel, M. N. Tahir, M. Khan, S. F. Adil, M. R. Shaik, M. Kuniyil, A. Al-Warthan and W. Tremel, *Dalton Trans.*, 2024, **53**, 3132–3142.
22 M. Tayyab, Y. Liu, S. Min, R. M. Irfan, Q. Zhu, L. Zhou, J. Lei and J. Zhang, *Chin. J. Catal.*, 2022, **43**, 1165–1175.
23 X. Gong, Q. Shi, M. S. Khalid, X. Gu, J. Li, L. Xu, B. Lumbers and G. Li, *ACS Appl. Nano Mater.*, 2024, **7**, 2062–2071.
24 A. L. Canepa, V. R. Elias, V. M. Vaschetti, E. V. Sabre, G. A. Eimer and S. G. Casuscelli, *Appl. Catal., A*, 2017, **545**, 72–78.
25 Q. Tang, Y. Chen and Y. Yang, *J. Mol. Catal. A: Chem.*, 2010, **315**, 43–50.
26 L. M. M. Correia, M. M. A. Soliman, C. M. Granadeiro, S. S. Balula, L. M. D. R. S. Martins, A. J. L. Pombeiro and E. C. B. A. Alegria, *Microporous Mesoporous Mater.*, 2021, **320**, 111111.
27 K. Otake, Y. Cui, C. T. Buru, Z. Li, J. T. Hupp and O. K. Farha, *J. Am. Chem. Soc.*, 2018, **140**, 8652–8656.
28 M. Mandal, C. J. Cramer, D. G. Truhlar, J. Sauer and L. Gagliardi, *ACS Catal.*, 2020, **10**, 10051–10059.
29 H. R. Tian, R. H. Li, J. Miao, S. X. Liu, F. F. Wang and Z. P. Zheng, *Dalton Trans.*, 2023, **52**, 9121–9130.
30 R. Q. Zhang, X. H. Song, Y. Y. Liu, P. Wang, Z. Y. Wang, Z. K. Zheng, Y. Dai and B. B. Huang, *J. Mater. Chem. A*, 2019, **7**, 26934–26943.
31 J. Zhong, Y. Shen, P. Zhu, S. Yao and C. An, *Nano Res.*, 2022, **16**, 202–208.
32 R. Li, P. Kuang, L. Wang, H. Tang and J. Yu, *J. Chem. Eng.*, 2022, **431**, 134137.
33 J. Wan, X. Mu, Y. Jin, J. Zhu, Y. Xiong, T. Li and R. Li, *Green Chem.*, 2022, **24**, 4870–4876.
34 J. K. Li, A. Wang, X. Y. Dong, S. Huang, Y. Meng and J. L. Song, *New J. Chem.*, 2023, **47**, 5970–5976.
35 M. Zhang, Z. Xu, B. Liu, Y. Duan, Z. Zheng, L. Li, Q. Zhou, V. G. Matveeva, Z. Hu, J. Yu and K. Yan, *AIChE J.*, 2023, **69**, e18077.
36 Y. Xu, H. Liu, Y. Wu, Q. Wu, C. Li, X. Wang, H. Qin, A. Qin and L. Wang, *ChemNanoMat*, 2023, **9**, e202300414.
37 J. K. Li, A. Wang, X. Y. Dong, S. Huang, M. Ye and J. L. Song, *Int. J. Hydrogen Energy*, 2024, **49**, 228–237.
38 L. Huang, X. Lin, K. Zhang, J. Zhang, C. Wang, S. Qu and Y. Wang, *Appl. Catal., B*, 2024, **346**, 123739.
39 S. Ghosh, J. N. Hausmann, L. Reith, G. Vijaykumar, J. Schmidt, K. Laun, S. Berendts, I. Zebger, M. Driess and P. W. Menezes, *Adv. Energy Mater.*, 2024, **14**, 2400356.
40 J. Li, J. Zhang, W. Gao, X. Cheng, X. Zhao, S. Gao, N. Shang and C. Wang, *Chem. Eng. Sci.*, 2024, **288**, 119813.
41 J. Bai, L. Chen, C. Lv, H. Ruo, Y. Pan, S. Xu, J. Chen, B. Yang, D. Zhang and H. Yang, *New J. Chem.*, 2024, **48**, 8436–8444.
42 C. Xiao, L. Zhang, H. Hao and W. Wang, *ACS Sustainable Chem. Eng.*, 2019, **7**, 7268–7276.
43 D. Feng, Y. Dong, L. Zhang, X. Ge, W. Zhang, S. Dai and Z. Qiao, *Angew. Chem., Int. Ed.*, 2020, **59**, 19503–19509.
44 E. Tiburcio, R. Greco, M. Mon, J. B. Soberanas, J. F. Soria, M. L. Haro, J. C. H. Garrido, J. O. Meseguer, C. Marini, M. Boronat, D. Armentano, A. L. Perez and E. Pardo, *J. Am. Chem. Soc.*, 2021, **143**, 2581–2592.
45 S. M. Zhang, Y. Wang, Y. Y. Ma, Z. B. Li, J. Du and Z. G. Han, *Inorg. Chem.*, 2022, **61**, 20596–20607.
46 Y. Li, X. Li, Z. An, Y. Chu and X. Wang, *Chem. – Asian J.*, 2023, **18**, e202300814.
47 G. Xu, L. Dai, M. Du, A. Peng, G. Zeng, H. Chen, R. Yan and W. Li, *ACS Sustainable Chem. Eng.*, 2024, **12**, 2741–2760.
48 L. Mohapatra and S. H. Yoo, *Mater. Today Energy*, 2023, **35**, 101331.
49 K. Gao, Y. Cheng, Z. Zhang, X. Huo, C. Guo, W. Fu, J. Xu, G. L. Hou, X. Shang and M. Zhang, *Angew. Chem., Int. Ed.*, 2024, **63**, e202319488.
50 C. Chen, G. Qiu, T. Wang, Z. Zheng, M. Huang and B. Li, *J. Colloid Interface Sci.*, 2021, **592**, 1–12.
51 Z. Zheng, F. Han, B. Xing, X. Han and B. Li, *J. Colloid Interface Sci.*, 2022, **624**, 460–470.
52 X. Han, W. Chen, M. Xu, T. Bai and B. Li, *Sep. Purif. Technol.*, 2024, **345**, 127397.
53 Y. Kon, T. Nakashima, S. Onozawa, K. Sato and S. Kobayashi, *Adv. Synth. Catal.*, 2022, **364**, 3372–3377.
54 A. Lieb, H. Leclerc, T. Devic, C. Serre, I. Margiolaki, F. Mahjoubi, J. S. Lee, A. Vimont, M. Daturi and J. S. Chang, *Microporous Mesoporous Mater.*, 2012, **157**, 18–23.
55 S. Mondal, P. Samanta, R. Sahoo, T. Kuila and M. C. Das, *J. Chem. Eng.*, 2023, **470**, 144340.
56 Y. Hou, H. Mao and L. Xu, *Nano Res.*, 2017, **10**, 344–353.
57 P. Bai, Z. Zhao, Y. Zhang, Z. He, Y. Liu, C. Wang, S. Ma, P. Wu, L. Zhao, S. Mintova and Z. Yan, *ACS Appl. Mater. Interfaces*, 2023, **15**, 19653–19664.
58 L. Zhang, R. Chen, Y. Tu, X. Gong, X. Cao, Q. Xu, Y. Li, B. Ye, Y. Ye and J. Zhu, *ACS Catal.*, 2023, **13**, 2202–2213.
59 H. Yuan, Q. Li, Z. Liu, Q. Qi, C. Wan, X. Yin, X. Yang, Y. Ding and Z. Du, *Appl. Catal., A*, 2023, **654**, 119070.
60 J. Luo, S. Yang, Y. Ling, W. Yang, H. Niu, W. Li, H. Liu and C. Liang, *J. Chem. Eng.*, 2023, **473**, 145171.
61 Z. Wang, B. Zhang, S. Yang, X. Yang, F. Meng, L. Zhai, Z. Li, S. Zhao, G. Zhang and Y. Qin, *J. Catal.*, 2022, **414**, 385–393.
62 J. Luo, Y. Zhou, S. Yang, W. Zhu, S. Li and C. Liang, *ACS Appl. Mater. Interfaces*, 2023, **15**, 22025–22035.
63 M. Yaghubzadeh, S. Alavinia and R. Ghorbani-Vaghei, *RSC Adv.*, 2023, **13**, 24639–24648.
64 S. Kumar, M. Kumar and V. Bhalla, *ACS Appl. Mater. Interfaces*, 2023, **15**, 49246–49258.
65 L. Liu, X. Zhou, C. Xin, B. Zhang, G. Zhang, S. Li, L. Liu and X. Tai, *RSC Adv.*, 2023, **13**, 23648–23658.
66 Q. Hao, Z. Li, Y. Shi, R. Li, Y. Li, L. Wang, H. Yuan, S. Ouyang and T. Zhang, *Angew. Chem., Int. Ed.*, 2023, **62**, e202312808.
67 J. Liu, H. Yang, U. I. Kara, E. Boerner, Y. Luo, H. Yu, Y. Xu, X. Wang and K. Huang, *J. Chem. Eng.*, 2024, **479**, 147778.

68 G. Zhong, D. Liu and J. Zhang, *Cryst. Growth Des.*, 2018, **18**, 7730–7744.
69 A. Vimont, J. M. Goupil, J. C. Lavalley, M. Daturi, S. Surblé, C. Serre, F. Millange, G. Férey and N. Audebrand, *J. Am. Chem. Soc.*, 2006, **128**, 3218.
70 J. W. Yoon, Y. K. Seo, Y. K. Hwang, J. S. Chang, H. Leclerc, S. Wuttke, P. Bazin, A. Vimont, M. Daturi, E. Bloch, P. L. Llewellyn, C. Serre, P. Horcajada, J. M. Grenèche, A. E. Rodrigues and G. Férey, *Angew. Chem., Int. Ed.*, 2010, **49**, 5949.
71 J. Tang and J. Wang, *Environ. Sci. Technol.*, 2018, **52**, 5367–5377.
72 A. Corma, H. García and F. X. Llabrés i Xamena, *Chem. Rev.*, 2010, **110**, 4606.

 